

# Discovery of Five Candidate Analogs for $\eta$ Carinae in Nearby Galaxies

Rubab Khan<sup>1,2,5</sup>, Scott M. Adams<sup>3</sup>, K. Z. Stanek<sup>3,4</sup>, C. S. Kochanek<sup>3,4</sup>, G. Sonneborn<sup>2</sup>

## ABSTRACT

The late-stage evolution of very massive stars such as  $\eta$  Carinae may be dominated by poorly understood episodic mass ejections which may later lead to superluminous supernovae. However, as long as  $\eta$  Car is one of a kind, it is nearly impossible to quantitatively evaluate these possibilities. Here we announce the discovery of five objects in the nearby ( $\sim 4\text{--}8$  Mpc) massive star-forming galaxies M 51, M 83, M 101 and NGC 6946 that have optical through mid-infrared photometric properties consistent with the hitherto unique  $\eta$  Car. We identified these  $L_{bol} \simeq 3\text{--}8 \times 10^6 L_{\odot}$  objects through a systematic search of archival *Spitzer* and HST data. Their *Spitzer* mid-infrared spectral energy distributions rise steeply in the  $3.6\text{--}8\text{ }\mu\text{m}$  bands, then turn over between  $8$  and  $24\text{ }\mu\text{m}$ , indicating the presence of warm ( $\sim 400\text{--}600$  K) circumstellar dust. Their optical counterparts or flux limits from deep HST images are  $\sim 1.5\text{--}2$  dex fainter than their mid-IR peaks and require the presence of  $\sim 5\text{--}10 M_{\odot}$  of obscuring material. Our finding implies that the rate of  $\eta$  Car-like events is a fraction  $f = 0.094$  ( $0.040 < f < 0.21$  at 90% confidence) of the core-collapse supernova rate.

*Subject headings:* stars: evolution, massive, mass-loss — stars: individual ( $\eta$  Carinae)

## 1. Introduction

The last stages of the evolution of the most massive ( $M \gtrsim 30 M_{\odot}$ ) stars may be dominated by episodic large mass-ejections (e.g., Humphreys & Davidson 1984). This leads to dust condensing out of the ejecta, obscuring the star in the optical but revealing it in the mid-infrared (mid-IR) as the absorbed UV and optical photons are re-emitted at longer wavelengths (e.g., Kochanek et al.

---

<sup>1</sup>NASA Goddard Space Flight Center, MC 665, 8800 Greenbelt Road, Greenbelt, MD 20771; rubab.m.khan, george.sonneborn-1@nasa.gov

<sup>2</sup>NASA Postdoctoral Program, ORAU, P.O. Box 117, MS 36, Oak Ridge, TN 37831

<sup>3</sup>Dept. of Astronomy, The Ohio State University, 140 W. 18th Ave., Columbus, OH 43210; sadams, kstanek, ckochanek@astronomy.ohio-state.edu

<sup>4</sup>Center for Cosmology and AstroParticle Physics, The Ohio State University, 191 W. Woodruff Ave., Columbus, OH 43210

<sup>5</sup>JWST Fellow

2012). The best known example is  $\eta$  Carinae ( $\eta$  Car) which contains one of the most massive ( $100\text{--}150 M_{\odot}$ ) and most luminous ( $\sim 5 \times 10^6 L_{\odot}$ ) stars in our Galaxy (e.g., Robinson et al. 1973). Its Great Eruption in the mid-1800s led to the ejection of  $\sim 10 M_{\odot}$  of material (Smith et al. 2003) now seen as a dusty nebula around the star. No Galactic or extragalactic analogs of this extraordinary laboratory for stellar astrophysics (in terms of stellar mass, luminosity, ejecta mass, time since mass ejection etc.) has previously been found.

A related puzzle is the existence of superluminous supernovae (SLSNe) that are plausibly explained by the SN ejecta colliding with a massive shell of previously ejected material (e.g., Smith & McCray 2007). A number of SN have also shown transients that could be associated with such ejections shortly prior to the final explosion (e.g., Pastorello et al. 2007; Ofek et al. 2013), although the relationship between these transients and  $\eta$  Car or other LBVs surrounded by still older, massive dusty shells (e.g., Smith & Owocki 2006) is unclear.

There are presently no clear prescriptions for how to include events like the Great Eruption into theoretical models. Even basic assumptions — such as whether the mass loss is triggered by the final post-carbon ignition phase as suggested statistically by Kochanek et al. (2012) or by an opacity phase-transition in the photosphere (e.g., Vink et al. 1999) or by interactions with a binary companion (e.g., Soker 2005) — are uncertain. Studies of possible mass-loss mechanisms (e.g., Owocki et al. 2004; Dessart et al. 2010; Smith & Arnett 2014; Shiode & Quataert 2014) are unfortunately non-prescriptive on either rate or outcome. Observationally, we are limited by the small numbers of high mass stars in this short evolutionary phase and searching for them in the Galaxy is complicated by having to look through the crowded, dusty disk and distance uncertainties. Obtaining a better understanding of this phase of evolution requires exploring other galaxies.

We demonstrated in Khan et al. (2010, 2011, 2013) that searching for extragalactic self-obscured stars utilizing *Spitzer* images is feasible, and in Khan et al. (2015a) we isolated an emerging class of 18 self-obscured stars with  $L_{bol} \sim 10^{5.5\text{--}6.0} L_{\odot}$  ( $M_{ZAMS} \simeq 25\text{--}60 M_{\odot}$ ) in galaxies at  $\sim 1\text{--}4$  Mpc. As the logical next step, we have now expanded our search to the large star-forming galaxies M 51, M 83, M 101 and NGC 6946 (distance  $\simeq 4\text{--}8$  Mpc). We picked these galaxies because they have high star-formation rates and are known to have hosted significant numbers (20, e.g., Botticella et al. 2012) of core-collapse supernovae (ccSNe) over the past century, indicating that they are likely to host a significant number of evolved high mass stars.

In this letter, we announce the discovery of five objects in these galaxies that have optical through mid-IR photometric properties consistent with the hitherto unique  $\eta$  Car as it is presently observed. In what follows, we describe our search method (Section 2), analyze the physical properties of the five potential  $\eta$  Car analogs (Section 3) and consider the implications of our findings (Section 4).

## 2. The $\eta$ Car Analog Candidates

At extragalactic distances, an  $\eta$  Car analog would appear as a bright, red point-source in *Spitzer* IRAC (Fazio et al. 2004) images, with a fainter optical counterpart due to self-obscuration. Given enough absorption, the optical counterpart could be undetectable. Building on our previous work (Khan et al. 2011, 2013, 2015a,b), we relied on these properties to identify the  $\eta$  Car analog candidates. For M 51 ( $D \simeq 8$  Mpc, Ferrarese et al. 2000), M 83 ( $D \simeq 4.61$  Mpc, Saha et al. 2006) and M 101 ( $D \simeq 6.43$  Mpc, Shappee & Stanek 2011) we used the full *Spitzer* mosaics available from the Local Volume Legacy Survey (LVL, Dale et al. 2009), and for NGC 6946 ( $D \simeq 5.7$  Mpc, Sahu et al. 2006) we used those from the *Spitzer* Infrared Nearby Galaxies Survey (SINGS, Kennicutt et al. 2003). We built Vega-calibrated IRAC  $3.6 - 8 \mu\text{m}$  and MIPS (Rieke et al. 2004)  $24 \mu\text{m}$  point-source catalogs for each galaxy following the procedures described in Khan et al. (2015b). We required  $> 3\sigma$  detection through PSF fitting of all cataloged sources at  $3.6$  and  $4.5 \mu\text{m}$ , complemented these measurements at  $5.8 \mu\text{m}$  through a combination of PSF and aperture photometry, and used only aperture photometry at  $8.0$  and  $24 \mu\text{m}$  as the PSF size and PAH emission both increase toward longer wavelengths.

To identify potential self-obscured massive-star candidates, we first fit the  $3.6 - 8 \mu\text{m}$  spectral energy distribution (SED) of each object to determine the slope  $a$  ( $\lambda L_\lambda \propto \lambda^a$ ). We then estimated the total IRAC luminosity ( $L_{\text{IR}}$ ) using the trapezoid rule integral of  $L_\lambda$  across the IRAC band centers as  $L_{\text{IR}} = \sum_{i=1}^3 \frac{1}{2} (\lambda_{i+1} - \lambda_i) (L_{\lambda_i} + L_{\lambda_{i+1}})$ , where  $\lambda_i = 3.6, 4.5, 5.8$ , and  $8.0 \mu\text{m}$ . We also calculated the fraction  $f$  of  $L_{\text{IR}}$  that is emitted in the first three IRAC bands. Following the selection criteria established in Khan et al. (2013) —  $L_{\text{IR}} > 10^5 L_\odot$ ,  $a > 0$  and  $f > 0.3$  — we initially selected  $\sim 700$  sources from our mid-IR point-source catalogs of the targeted galaxies.

We examined the IRAC image locations of the selected sources to exclude those associated with saturated, resolved or unambiguously foreground objects, and utilized the Vizier<sup>1</sup> web-service to rule out spectroscopically confirmed non-stellar sources and those known to have high proper motions consistent with Galactic sources. We visually inspected the  $3.6 - 24 \mu\text{m}$  SEDs of the remaining sources to identify the ones that most closely resemble the SED of  $\eta$  Car and then queried the Hubble Source Catalog (HSC<sup>2</sup>, Version 1) to exclude those with bright optical counterparts ( $m \lesssim 20$ , implying  $L_{\text{opt}} \gtrsim 1.5 - 6 \times 10^5 L_\odot$ ). These steps produced a short-list of  $\sim 20$  sources for which we retrieved all publicly available archival HST images along with the associated photometry from the Hubble Legacy Archive (HLA<sup>3</sup>). Since the HST and *Spitzer* images sometimes have significant ( $\sim 1''$ ) astrometric mismatches, we utilized the IRAF GEOMAP and GEOXYTRAN tasks to locally align the HST and *Spitzer* images with uncertainties  $\lesssim 0''.1$ . We then identified the closest optical counterpart within a matching radius of  $0''.3$ .

---

<sup>1</sup><http://vizier.u-strasbg.fr/>

<sup>2</sup><https://archive.stsci.edu/hst/hsc/search.php>

<sup>3</sup><http://hla.stsci.edu/>

We identified five sources with mid-IR SEDs closely resembling that of  $\eta$  Car and optical fluxes or flux limits  $\sim 1.5 - 2$  dex fainter than their mid-IR peaks. We will refer to these sources as  $\eta$  Twins-1, 2, 3, 4 and 5. We find one source each in M 51 ( $\eta$  Twin-1), M 101 ( $\eta$  Twin-2) and NGC 6946 ( $\eta$  Twin-3), and two sources in M 83 ( $\eta$  Twins-4, 5). We identified HST counterparts of  $\eta$  Twins-1, 2, 4 and 5 and verified that none of the other cataloged sources within the matching radius would be a more logical photometric match (brighter and redder). No HST counterpart of  $\eta$  Twin-3 was found within the  $0''.3$  matching radius and we adopted the fluxes of the nearest cataloged source at  $0''.85$  as the upper flux limits for this object. Table 1 lists the coordinates and optical through mid-IR fluxes of these five sources, Figure 1 shows their IRAC  $3.6\mu\text{m}$  and HST  $I$ -band (F814W) images, and Figure 2 shows their SEDs.  $\eta$  Twins-1, 4 and 5 are  $\text{H}\alpha$  emitters and  $\eta$  Twin-2 is a UV source (see Table 1).

We have  $UBVR$  variability data for M 51, M 101 and NGC 6946 from the LBC survey for failed supernovae (Kochanek et al. 2008; Gerke et al. 2014). We analyzed 21/26/37 epochs of data spanning a 7.1/7.2/8 year period for M 51/M 101/NGC 6946 with the ISIS image subtraction package (Alard & Lupton 1998). We did not detect any significant optical variability at the locations of  $\eta$  Twins-1, 2 or 3.

Cutri et al. (2012) identified  $\eta$  Twin-2 as a WISE point source and we use their  $12\mu\text{m}$  flux measurement as an upper limit for SED models (Section 3). We also note that Grammer & Humphreys (2013) do not list the HST counterpart of  $\eta$  Twin-2 as a luminous star. Johnson et al. (2001) reports an optically thick free-free radio source located  $0''.49$  from  $\eta$  Twin-3 and Hadfield et al. (2005) identified a source with Wolf-Rayet spectroscopic signature  $1''.54$  from  $\eta$  Twin-4. We could not confirm if these sources are reasonable astrometric matches to the IRAC locations.  $\eta$  Twins-4 and 5 were cataloged as mid-IR point sources by Williams et al. (2015), but they flagged neither as massive stars.

### 3. SED Modeling

Following the procedures from Khan et al. (2011, 2015a), we fit the SEDs of these five sources using DUSTY (Ivezic & Elitzur 1997; Elitzur & Ivezić 2001) to model radiation transfer through a spherical medium surrounding a blackbody source, which is also a good approximation for a combination of unresolved non-spherical /patchy /multiple circumstellar shells. We considered models with either graphitic or silicate dust (Draine & Lee 1984). The models are defined by the stellar luminosity ( $L_*$ ), stellar temperature ( $T_*$ ),  $V$ -band optical depth ( $\tau_V$ ), dust temperature at the inner-edge of the shell ( $T_d$ ) and shell thickness  $\zeta = R_{out}/R_{in}$ . We embedded DUSTY inside a Markov Chain Monte Carlo (MCMC) driver to fit each SED by varying  $T_*$ ,  $\tau_V$ , and  $T_d$  with  $L_*$  determined by a  $\chi^2$  fit for each model. We fixed  $\zeta = 4$ , since its exact value has little effect on the results (Khan et al. 2015a) and limited  $T_*$  to a maximum value of  $\sim 50,000$  K.

The best fit model parameters determine the radius of the inner edge of the stellar-ejecta

distribution ( $R_{in}$ ). The mass of the shell is  $M_e = 4\pi R_{in}^2 \tau_V / \kappa_V$  (scaled to a visual opacity of  $\kappa_V = 100 \kappa_{v100} \text{ cm}^2/\text{g}$ ) and the age estimate for the shell is  $t_e = R_{in}/v_e$  (scaled as  $v_e = 100 v_{e100} \text{ km s}^{-1}$ ) where we can ignore  $R_{out}$  to zeroth order. Table 2 reports the parameters of the best fit models for both dust types, and Figure 2 shows the best fit models for each source. We also fit models using Castelli & Kurucz (2004) stellar atmosphere models instead of blackbodies. Since these resulted in similar parameter estimates, we only report the blackbody results in Figure 2 and Table 2.

Comparing the best fit models derived for both dust types shows that the integrated luminosity estimates depend little on the choice of dust type, and are in the range of  $L_* \simeq 10^{6.5-6.9} L_\odot$ . For  $\eta$  Twins-2, 4 and 5, the stellar temperature estimates reach the allowed maximum of  $\sim 50,000 \text{ K}$ , indicating the presence of at least one very hot star. The best fit models of  $\eta$  Twin-1 also require the presence of a hot star, but with temperatures lower than the allowed maximum:  $\sim 29,000 \text{ K}$  for graphitic and  $\sim 43,000 \text{ K}$  for silicate dust. Constrained by the optical upper flux limits, the best fit models of  $\eta$  Twin-3 require the presence of a cool star with  $T_* \simeq 5,000 \text{ K}$  for either dust type, although forcing the models to trace each of the flux limits would require a hot star model.

Generally, the best fits derived for graphitic dust require lower optical depths, lower dust temperatures and larger shell radii, leading to higher ejecta masses and age estimates. For  $\eta$  Twins-2 and 4, the best fits derived for graphitic dust had lower  $\chi^2$ , and for  $\eta$  Twin-5 the best fits for both dust types have nearly identical  $\chi^2$ . For  $\eta$  Twins-1 and 3, the best fits derived for silicate dust have lower  $\chi^2$ , and those derived for graphitic dust require essentially unphysical ejecta masses. Considering the best fit graphitic models for  $\eta$  Twins-2, 4 and 5 and the best fit silicate models for  $\eta$  Twins-1,a and 3 (shown on Figure 2), the five  $\eta$  Car analog candidates appear to be embedded in  $\sim 5 - 10 M_\odot$  of warm ( $\sim 400 - 600 \text{ K}$ ) obscuring material ejected a few centuries ago.

Figure 3 contrasts the bolometric luminosities and ejecta mass estimates of these five objects with the relatively less luminous self-obscured stars we identified in Khan et al. (2015a). The five new sources form a distinct cluster close to  $\eta$  Car in the  $L_{bol} - M_{ejecta}$  parameter space, whereas the previously identified stars are more similar to the Galactic OH/IR star IRC+10420 (e.g., Tiffany et al. 2010) or M 33’s Variable A (e.g., Humphreys et al. 1987).

#### 4. Discussion

To an extragalactic observer located in one of the targeted galaxies surveying the Milky Way with telescopes similar to the HST and *Spitzer*,  $\eta$  Car’s present day SED would appear identical to the extragalactic  $\eta$  Car analog candidates we found. The Carina nebula is  $\sim 2.5^\circ$  in extent (Smith & Brooks 2007) corresponding to  $\sim 2''.5$  at our most distant galaxy (M 51 at 8 Mpc). While this would not be resolved by *Spitzer*, we showed in Khan et al. (2013) that we can distinguish between the mid-IR SED of an unresolved analog of the Carina nebula hosting an  $\eta$  Car from one lacking an  $\eta$  Car. More importantly, a  $\sim 2''.5$  stellar complex would be easily resolved by HST.

Because clusters more compact than the Carina Nebula are not uncommon, in Khan et al.

(2013) we considered whether dusty clusters can hide  $\eta$  Car like stars and if we would confuse unresolved star-clusters with  $\eta$  Car analogs. In general, a cluster sufficiently luminous to hide an evolved  $\gtrsim 30 M_{\odot}$  star has hosted many luminous stars with strong UV radiation fields and winds, which will generally clear the cluster of the gas and dust needed to produce strong mid-IR emission over the timescale that even the most massive star needs to evolve away from the main sequence. Moreover, emission from warm circumstellar ejecta peaks between the IRAC  $8 \mu\text{m}$  and MIPS  $24 \mu\text{m}$  bands and then turns over, as seen in all of our candidates, unlike emission from colder intra-cluster dust that generally peaks at longer wavelengths.

A significant majority of massive stars are expected to be in multiple-star systems (e.g., Mason et al. 2009; Sana & Evans 2011), as is the case for  $\eta$  Car (e.g., Verner et al. 2005; Mehner et al. 2010). This is a minor complication, affecting luminosity estimates by at most a factor of 2, and mass estimates even less. If we expand our simple rate estimates from Khan et al. (2015a) assuming that the candidates we have identified are real analogs of  $\eta$  Car, then our galaxy sample (including the Milky Way) contains  $N_c = 6$   $\eta$  Car-like stars, implying an eruption rate over the 12 galaxies of  $F_e = 0.033 t_{d200}^{-1} \text{yr}^{-1}$  ( $0.016 \text{yr}^{-1} < F_e t_{d200} < 0.059 \text{yr}^{-1}$  at 90% confidence) where  $t_d \simeq 200$  yrs is a rough estimate of the period over which our method would detect an  $\eta$  Car-like source. For comparison, the estimated star formation rate for the sample is  $SFR_{H\alpha} \simeq 10 M_{\odot}/\text{yr}$  (mainly based on Kennicutt et al. 2008) and the number of SN recorded over the past 30 years is 10 for an SN rate of  $F_{SN} = 0.33/\text{yr}$  (26 over the past century, mainly based on Botticella et al. 2012). For  $N_c = 6$ ,  $t_d \simeq 200$  yrs, and  $N_{SN} = 10$  over  $t_{SN} = 30$  yrs, this implies that the rate of  $\eta$  Car-like events is a fraction  $f = 0.094$  ( $0.040 < f < 0.21$  at 90% confidence) of the ccSNe rate.

We identified the five potential  $\eta$  Car analogs through a systematic search, specifically focusing on finding sources that most closely resemble the SED of present day  $\eta$  Car. The reason that the SEDs of these five sources are so remarkably similar to each other is by design. We have not closely studied the less luminous mid-IR sources that may belong to the class of self-obscured stars we identified in Khan et al. (2015a), and some of the sources that we excluded because they have relatively bright optical counterparts may indeed be evolved high mass stars with older, lower optical-depth shells. It is readily apparent from this discussion that a closer scrutiny of our mid-IR catalogs would reveal richer and more diverse populations of evolved massive stars. This in turn will let us better quantify the abundance of those stars, and constrain the rates of mass ejection episodes and mass loss from massive stars prior to their death by core-collapse.

The  $\eta$  Car analog candidates we identified can be studied at greater detail with the James Webb Space Telescope (JWST, e.g., Gardner et al. 2006), taking advantage of its order-of-magnitude-higher spatial resolution. These sources are luminous in the  $3.6 - 24 \mu\text{m}$  wavelength range where the JWST will be most sensitive. They are rare laboratories for stellar astrophysics and will be very interesting extragalactic stellar targets for spectroscopic study with JWST’s mid-IR instrument (MIRI, Rieke et al. 2015). This will give us an unprecedented view of these most-massive self-obscured stars, letting us study their evolutionary state and the composition of their circumstellar ejecta.

RK is supported by a JWST Fellowship awarded through the NASA Postdoctoral Program. SMA is supported by a Presidential Fellowship at The Ohio State University. KZS is supported in part by NSF Grant AST-151592. CSK is supported by NSF grant AST-1515876. This research has made use of observations made with the *Spitzer* Space Telescope, which is operated by the JPL and Caltech under a contract with NASA; observations made with the NASA/ESA Hubble Space Telescope and obtained from the Hubble Legacy Archive, which is a collaboration between the STScI/NASA, ST-ECF/ESA and the CADC/NRC/CSA; and the VizieR catalog access tool, CDS, Strasbourg, France.

## REFERENCES

- Alard, C. & Lupton, R. H. 1998, *ApJ*, 503, 325
- Botticella, M. T., Smartt, S. J., Kennicutt, R. C., et al. 2012, *A&A*, 537, A132
- Castelli, F., & Kurucz, R. L. 2004, arXiv:astro-ph/0405087
- Cutri, R. M. et al. 2012, VizieR Online Data Catalog, 2311, 0
- Dale, D. A. et al. 2009, *ApJ*, 703, 517
- Dessart, L., Livne, E., & Waldman, R. 2010, *MNRAS*, 405, 2113
- Draine, B. T. & Lee, H. M. 1984, *ApJ*, 285, 89
- Elitzur, M. & Ivezić, Ž. 2001, *MNRAS*, 327, 403
- Fazio, G. G. et al. 2004, *ApJS*, 154, 10
- Ferrarese, L., Mould, J. R., Kennicutt, R. C., Jr., et al. 2000, *ApJ*, 529, 745
- Gardner, J. P. et al. 2006, *SSR*, 123, 485
- Gerke, J. R., Kochanek, C. S., & Stanek, K. Z. 2015, *MNRAS*, 450, 3289
- Grammer, S., & Humphreys, R. M. 2013, *AJ*, 146, 114
- Hadfield, L. J., Crowther, P. A., Schild, H., & Schmutz, W. 2005, *A&A*, 439, 265
- Humphreys, R. M. & Davidson, K. 1984, *Science*, 223, 243
- Humphreys, R. M., Jones, T. J., & Gehrz, R. D. 1987, *AJ*, 94, 315
- Ivezic, Z. & Elitzur, M. 1997, *MNRAS*, 287, 799
- Johnson, K. E., Kobulnicky, H. A., Massey, P., & Conti, P. S. 2001, *ApJ*, 559, 864

- Kennicutt, Jr., R. C. et al. 2003, *PASP*, 115, 928
- . 2008, *ApJS*, 178, 247
- Khan, R. et al. 2010, *ApJ*, 715, 1094
- Khan, R., Stanek, K. Z., Kochanek, C. S., & Bonanos, A. Z. 2011, *ApJ*, 732, 43
- Khan, R., Stanek, K. Z., & Kochanek, C. S. 2013, *ApJ*, 767, 52
- Khan, R., Kochanek, C. S., Stanek, K. Z., & Gerke, J. 2015a, *ApJ*, 799, 187
- Khan, R., Stanek, K. Z., Kochanek, C. S., & Sonneborn, G. 2015b, *ApJS*, 219, 42
- Kochanek, C. S. et al. 2008, *ApJ*, 684, 1336
- Kochanek, C. S., Szczygieł, D. M., & Stanek, K. Z. 2012, *ApJ*, 758, 142
- Mason, B. D., Hartkopf, W. I., Gies, D. R., Henry, T. J., & Helsel, J. W. 2009, *AJ*, 137, 3358
- Mehner, A., Davidson, K., Ferland, G. J., & Humphreys, R. M. 2010, *ApJ*, 710, 729
- Ofek, E. O. et al. 2013, *Nature*, 494, 65
- Owocki, S. P., Gayley, K. G., & Shaviv, N. J. 2004, *ApJ*, 616, 525
- Pastorello, A. et al. 2007, *Nature*, 447, 829
- Rieke, G. H. et al. 2004, *ApJS*, 154, 25
- Rieke, G. H., Wright, G. S., Böker, T., et al. 2015, *PASP*, 127, 584
- Robinson, G., Hyland, A. R., & Thomas, J. A. 1973, *MNRAS*, 161, 281
- Saha, A. et al. 2006, *ApJS*, 165, 108
- Sahu, D. K. et al. 2006, *MNRAS*, 372, 1315
- Sana, H., & Evans, C. J. 2011, *IAU Symposium*, 272, 474
- Shappee, B. J., & Stanek, K. Z. 2011, *ApJ*, 733, 124
- Shiode, J. H., & Quataert, E. 2014, *ApJ*, 780, 96
- Smith, N., Gehrz, R. D., Hinz, P. M., et al. 2003, *AJ*, 125, 1458
- Smith, N. & Owocki, S. P. 2006, *ApJ*, 645, L45
- Smith, N. & Brooks, K. J. 2007, *MNRAS*, 379, 1279
- Smith, N. & McCray, R. 2007, *ApJ*, 671, L17



- Smith, N., & Arnett, W. D. 2014, *ApJ*, 785, 82
- Soker, N. 2005, *ApJ*, 619, 1064
- Tiffany, C., Humphreys, R. M., Jones, T. J., & Davidson, K. 2010, *AJ*, 140, 339
- Verner, E., Bruhweiler, F., & Gull, T. 2005, *ApJ*, 624, 973
- Vink, J. S., de Koter, A., & Lamers, H. J. G. L. M. 1999, *A&A*, 350, 181
- Williams, S. J., Bonanos, A. Z., Whitmore, B. C., Prieto, J. L., & Blair, W. P. 2015, *A&A*, 578, A100

Table 1: Multi-Wavelength Photometry

	$\eta$ Twin-1	$\eta$ Twin-2	$\eta$ Twin-3	$\eta$ Twin-4	$\eta$ Twin-5
Host	M 51	M 101	NGC 6946	M 83	M 83
RA (deg)	202.46287	210.80203	308.76548	204.21782	204.21523
Dec (deg)	47.21126	54.31891	60.18314	−29.88722	−29.87481
$m_{UV}$	...	$23.25 \pm 0.05$	...	...	...
$m_U$	24.34	$23.16 \pm 0.03$	...	$22.27 \pm 0.02$	$21.70 \pm 0.02$
$m_B$	25.14	$24.26 \pm 0.03$	$> 24.01 \pm 0.05$	$23.31 \pm 0.02$	$22.67 \pm 0.02$
$m_V$	$23.64 \pm 0.06$	$23.92 \pm 0.03$	$> 23.62 \pm 0.05$	...	...
$m_{H\alpha}$	$18.26 \pm 0.01$	...	...	$22.00 \pm 0.06$	$22.38 \pm 0.09$
$m_R$	$21.90 \pm 0.03$	...	...	...	...
$m_I$	$22.31 \pm 0.08$	$23.23 \pm 0.03$	$> 22.74 \pm 0.06$	$22.58 \pm 0.03$	$22.25 \pm 0.03$
$m_{3.6}$	$14.68 \pm 0.12$	$15.08 \pm 0.11$	$14.45 \pm 0.11$	$14.26 \pm 0.10$	$14.59 \pm 0.12$
$m_{4.5}$	$14.10 \pm 0.06$	$13.97 \pm 0.04$	$14.20 \pm 0.06$	$13.79 \pm 0.07$	$14.30 \pm 0.09$
$m_{5.8}$	$12.20 \pm 0.05$	$11.99 \pm 0.06$	$11.47 \pm 0.09$	$11.40 \pm 0.08$	$11.54 \pm 0.09$
$m_{8.0}$	$10.38 \pm 0.10$	$10.12 \pm 0.01$	$9.84 \pm 0.06$	$9.70 \pm 0.11$	$9.95 \pm 0.07$
$m_{12}$	...	$> 8.81 \pm 0.06$	...	...	...
$m_{24}$	$6.50 \pm 0.20$	$7.07 \pm 0.02$	$6.09 \pm 0.13$	$6.09 \pm 0.20$	$6.47 \pm 0.05$

Vega magnitudes of the sources where the specific HST filters are UV:F275W;  $U$ :F336W,  $B$ :F435W ( $\eta$  Twin-2) / F438W (4, 5) / F439W (1) / F450W (3);  $V$ :F555W,  $H\alpha$ :F656N ( $\eta$  Twin-1) / F657N (3, 4),  $R$ :F675W,  $I$ :F814W. The HLA catalog reports no uncertainties for the U/B magnitudes of  $\eta$  Twin-1. The HST data sources are:  $\eta$  Twin-1: Prop. ID 7375 (PI: Scoville);  $\eta$  Twin-2: Prop. ID 9490 (PI: Kuntz) and Prop. ID 13364 (PI: Calzetti);  $\eta$  Twin-3: Prop. ID 9073 (PI: Bregman);  $\eta$  Twins-4, 5: Prop. ID 12513 (PI: Blair).

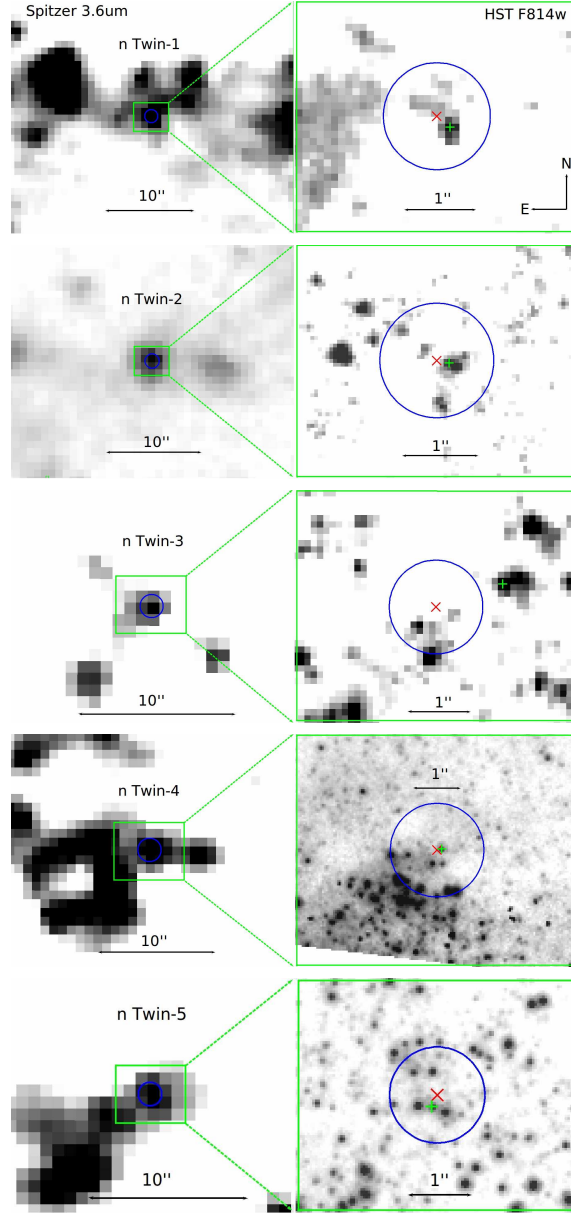


Fig. 1.— *Spitzer* IRAC  $3.6\,\mu\text{m}$  (left column) and HST *I*-band (F814W, right column) images of the candidate  $\eta$  Car analogs. The HST images were taken with ACS ( $\eta$  Twin-1), WFPC2 (2, 3) and WFC3 (4, 5). The circles are  $1''.5$  in diameter, which is roughly equal to the IRAC  $3.6\,\mu\text{m}$  PSF FWHM. The rectangles on the left column enclose the regions shown on the right column. On the HST images, “ $\times$ ” marks the location of the IRAC source (center of the circle) determined through pixel-to-pixel mapping as discussed in Section 2 and “+” marks the location of the closest cataloged HST source. For  $\eta$  Twin-3, the “+” marked source at  $0''.85$  was used to determine upper flux limits as the closer ( $> 0''.3$  &  $< 0''.85$ ) locations of optical flux excess were not identified as point-sources in the HLA catalog. North is up and east is left on all images. The scales on the IRAC images are  $10''.0$  and those on the HST images are  $1''.0$ .

Table 2: Best Fit SED Models

ID	$\chi^2/(m+n)$	$\tau_V$	$T_d$ (K)	$T_*$ (K)	$\log(R_{in})$ (cm)	$\log L_{bol}$ ( $L_\odot$ )	$M_e$ ( $M_\odot$ )	$t_e$ (years)
<i>Graphitic</i>								
$\eta$ Twin-1	156/(10 + 0)	4.27	384	29,000	17.56	6.863	35.12	1148
$\eta$ Twin-2	92/(10 + 1)	2.49	402	50,110	17.38	6.554	9.04	762
$\eta$ Twin-3	91/(5 + 3)	24.51	350	5,090	17.36	6.881	81.46	729
$\eta$ Twin-4	114/(8 + 0)	2.29	388	50,060	17.42	6.570	10.01	837
$\eta$ Twin-5	139/(8 + 0)	1.72	383	50,030	17.39	6.495	6.61	784
<i>Silicate</i>								
$\eta$ Twin-1	114/(10 + 0)	6.03	582	42,910	17.03	6.932	4.32	338
$\eta$ Twin-2	205/(10 + 1)	4.21	644	50,110	16.78	6.569	0.97	192
$\eta$ Twin-3	68/(5 + 3)	29.3	432	4,900	16.69	6.832	4.52	157
$\eta$ Twin-4	153/(8 + 0)	4.13	582	50,110	16.88	6.626	1.48	239
$\eta$ Twin-5	137/(8 + 0)	3.29	561	50,110	16.87	6.560	1.13	235

The format  $\chi^2/(m+n)$  indicates the goodness of fit  $\chi^2$ , the number of flux measurements  $m$  used to determine the luminosity and the number of upper limits  $n$  added to the estimate of  $\chi^2$  once the luminosity is determined. The remaining columns list the  $V$ -band optical depth ( $\tau_V$ ) of the shell, the temperature at the inner-edge of the shell ( $T_d$ ), the stellar temperature ( $T_*$ ), the shell thickness  $R_{out}/R_{in}$ , the bolometric luminosity ( $L_{bol}$ ), the estimated mass of the shell  $M_e = 4\pi R_{in}^2 \tau_V / \kappa_V$  (scaled as  $\kappa_V = 100 \kappa_{v100} \text{ cm}^2/\text{g}$ ) and an age estimate for the shell  $t_e = R_{in}/v_e$  (scaled as  $v_e = 100 v_{e100} \text{ km s}^{-1}$ ).

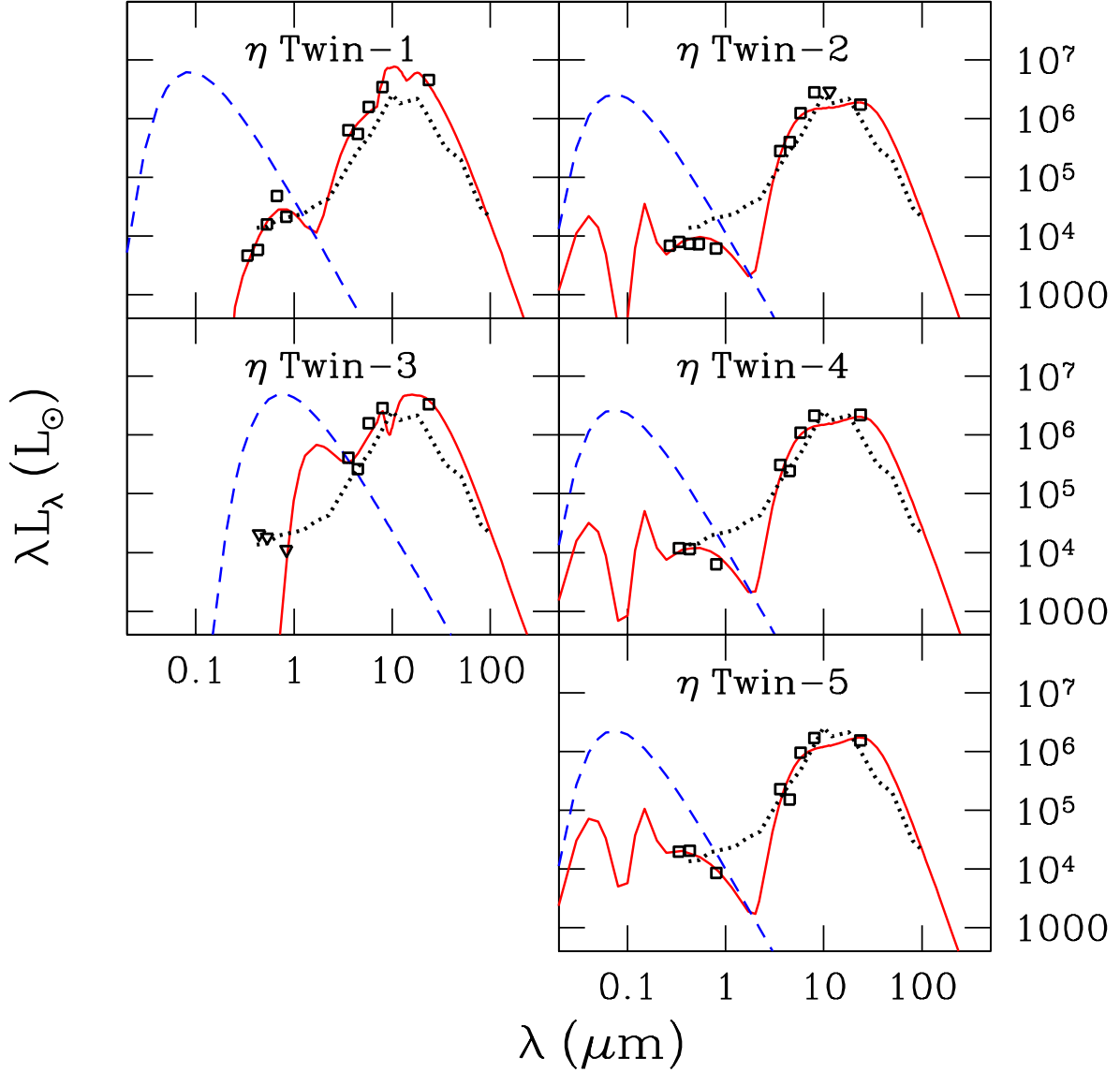


Fig. 2.— The best fit models (solid line) for the observed SEDs (squares and triangles with the latter for upper limits) of the candidate  $\eta$  Car analogs and the SEDs of the underlying, unobscured blackbody sources (dashed line), as compared to the SED of  $\eta$  Car (dotted line, from Robinson et al. 1973). Here we show the best fit silicate models for  $\eta$  Twins-1 and 3, and the best fit graphitic models for  $\eta$  Twins-2, 4 and 5 (see Section 3 and Table 2).

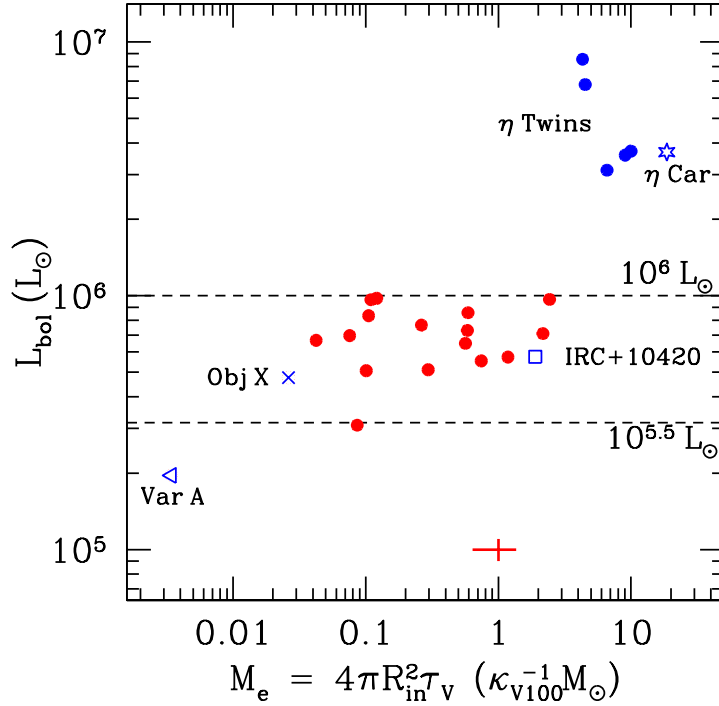


Fig. 3.— The luminosities,  $L_{bol}$ , of the candidate  $\eta$  Car analogs (blue circles) as a function of the ejecta mass estimates,  $M_e = 4\pi R_{in}^2 \tau_V / \kappa_V$ , compared to the less luminous (red circles) self-obscured stars we identified in Khan et al. (2015a). The Galactic OH/IR star IRC+10420 (e.g., Tiffany et al. 2010, square), M 33’s Variable A (e.g., Humphreys et al. 1987, triangle) and  $\eta$  Car (star symbol) are also shown for comparison. The error bar corresponds to the typical  $1\sigma$  uncertainties on  $L_{bol}$  ( $\pm 10\%$ ) and  $M_e$  ( $\pm 35\%$ ) of the best SED fit models.